SMAALEN, S. VAN (1994). Private communications.
SUENO, S., KIMATA, M. & OHMASA, M. (1979). *Modulated Structures*, edited by J. M. COWLEY, J. B. COHEN, M. B. SALAMON & B. J. WUENSCH. *AIP Conf. Proc.* **53**, 333–335.
VAN TENDELOO, G., GREGORIADES, P. & AMELINCKX, S. (1983). *J. Solid State Chem.* **50**, 321–334, 335–361.
VOGELS, L. J. P., BALZUWEIT, K., MEEKES, H. & BENNEMA, P. (1992). *J. Cryst. Growth*, **116**, 397–413.
VOGELS, L. J. P., VERHEIJEN, M. A., MEEKES, H. & BENNEMA, P. (1992). *J. Cryst. Growth*, **121**, 697–708.
WOLFF, P. M. DE, JANSSEN, T. & JANNER, A. (1981). *Acta Cryst.* A**37**, 625–636.

Acta Cryst. (1995). A**51**, 739–746

Maximum-Entropy Analysis of the Cubic Phases of KOH and KOD, NaOH and NaOD

BY KLAUS-DIETER SCHOTTE

Institut Theoretisch Physik, Freie Universität Berlin, Arnimallee 14, 14195 *Berlin, Germany*

URSULA SCHOTTE* AND HANS-JÜRGEN BLEIF

BENSC, Hahn-Meitner Institut, Glienicker Strasse 100, 14109 *Berlin, Germany*

AND ROBERT PAPOULAR

Brookhaven National Laboratory, Upton, New York 11973-5000, *USA*

(*Received* 14 *November* 1994; *accepted* 7 *April* 1995)

Dedicated to Professor W. Prandl on the occasion of his 60th birthday

Abstract

The maximum-entropy method (MEM) for structure determination is applied on the plastically crystalline phases of KOH and KOD characterized by delocalized H^+ or D^+ ions in a simple rock salt structure. The structure factors measured by neutron diffraction already give a consistent picture of the hydrogen distribution by conventional Fourier and modelling methods, which helps to understand the merit of the MEM. Owing to the negative sign of the scattering length of hydrogen, the MEM can, in a limited sense 'model free', separate off the hydrogen density distribution. It is found, however, that the MEM cannot be applied naively for these compounds and reasons are given why the uniform density as *a priori* information has to be given up in the present case. The *a priori* information procedure to be used is discussed. In addition, and perhaps unexpectedly, the deuterium density is also obtained.

1. Introduction

The high-temperature phases of the potassium and sodium hydroxides have sodium chloride structure and are plastic crystals with the H atom moving more or less freely in the vicinity of the O atom (Smit, Dachs & Lechner, 1979; Bleif & Dachs, 1982; Kara, 1982). Obvious questions are: does the OH group behave like a rigid dumb-bell jumping between favourable orientations or is there hydrogen bonding O—H—O or even diffusion of protons to make these compounds ionic conductors (El'kin, 1990)? Are the answers, linked to determining the OH distance, extractable from neutron or X-ray diffraction data?

With conventional methods, the structure determination would be tackled by modelling the anisotropic hydrogen distribution and extracting the Debye–Waller (DW) factors from the fit. For these plastic crystals, the DW factors are very large since the cubic phase is stable only in a temperature region around 550 K. Therefore, there are relatively few measurable reflections and Fourier methods should be reliable, *i.e.* cut-off effects from setting the intensity of unmeasured structure factors to zero should be small. The hydrogen distribution, however, gives rather small contributions to the structure factors and is not easy to separate. The procedure by 'different Fourier analysis' relies heavily on modelling. This, together with the lucky circumstance that all phases are known (they are all +1), makes the system an interesting candidate to test the maximum-entropy method (MEM), recently much propagated as a model-free method for crystallographic structure determination (see, for example, Sakata, Mori, Kumazawa, Takata & Toraya, 1990; Papoular, Prandl & Schiebel, 1992).

It seems one has a chance to find a realistic model-free hydrogen distribution using the fact that hydrogen has a

* Also at Mineralogisch-Petrographisches Institut, Universität Kiel, Germany.

Table 1. *Structure factors from single-crystal neutron diffraction for* KOH *and* KOD

Data from Kabs (1980); for NaOH the data (Bleif, 1978) are available on request. The lattice constant is $a_{KOH} = 5.76$ Å and the space group *Fm3m*. The scattering lengths are (in units of 10^{-12} cm) $b_K = 0.37$, $b_O = 0.58$, $b_D = 0.667$ and $b_H = -0.376$. $F(000)$, although not measurable, is four times the sum of the scattering lengths and consistent with the scaled experimental data.

h	k	l	F_{KOH}	σ	F_{KOD}	σ
1	1	1	0.17	0.05	2.21	0.06
2	0	0	2.49	0.03	3.81	0.08
2	2	0	2.22	0.02	2.65	0.04
3	1	1	0.76	0.02	0.49	0.02
2	2	2	1.81	0.02	2.01	0.03
4	0	0	1.63	0.02	1.01	0.02
3	3	1	0.52	0.02	0.50	0.02
4	2	0	1.17	0.02	1.03	0.03
4	2	2	0.92	0.02	0.99	0.03
5	1	1	0.45	0.02	0.25	0.06
3	3	3	0.36	0.02	0.59	0.04
4	4	0	0.48	0.02	0.75	0.06
5	3	1	0.20	0.06	0.33	0.02
6	0	0	0.39	0.03	0.53	0.05
4	4	2	0.33	0.03	0.69	0.04
6	2	0	0.34	0.03	0.44	0.04
5	3	3	0.12	0.07	0.30	0.04
6	2	2	0.17	0.04	0.41	0.05
4	4	4	—	—	0.44	0.04
7	1	1	—	—	0.27	0.05
6	4	0	—	—	0.27	0.06

negative neutron scattering length: Sakata, Uno, Takata & Howard (1993) used a modified MEM program (*MEND*; Kumazawa, Kubota, Takata & Sakata, 1993) where the positive and negative densities can be separated, which they successfully used first for TiO_2, where Ti has a negative scattering length. Similar ideas have been used for the determination of magnetic moment distributions (Papoular & Gillon, 1990).

Since the aim of this paper is mainly methodological, we restrict the discussion here to the potassium compounds KOH and KOD and give the results for sodium hydroxide only at the end, for comparison. We start in §2 with a short description of the conventional structure determination results to be used as a guideline when judging results obtained by the MEM. The details of the structure and dynamics of the plastically crystalline phases of the alkali hydroxides are being published in a separate paper. In §3 we apply the *MEED* (Sakata & Sato, 1990) and *MEND* programs. *MEED* was originally developed for X-ray and *MEND* for neutron diffraction data. Our results and conclusions are discussed in §4. Essentially, we find that for our system the programs must not be applied naively, that is with 'zero bias' or uniform density as *a priori* information.

2. Structure information from conventional modelling

The available structure amplitudes for KOH and KOD (Kabs, 1980) measured by neutron diffraction, together with standard deviations, are listed in Table 1. The density distribution of KOD

$$\rho(\mathbf{r}) = a^{-3} \sum_{n=1}^{N} F_{obs}(\mathbf{q}_n) \exp(i\mathbf{q}_n\mathbf{r}), \qquad (1)$$

where a is the lattice constant, is shown in Fig. 1. Since the structure factors F_{obs} were all chosen positive, the strongest peak appears at the origin; this corresponds to the O ion, whereas the K ion is at $0\frac{1}{2}0$. Fig. 1(*b*) shows cuts of the contour plot in [100] and [110] directions. Cut-off effects producing negative densities are seen to be small. One clearly sees the anisotropy of the D distribution while those of K and O are spherically isotropic.

For the latter, a simple Debye–Waller (DW) fit should be sufficient, while the hydrogen density can be

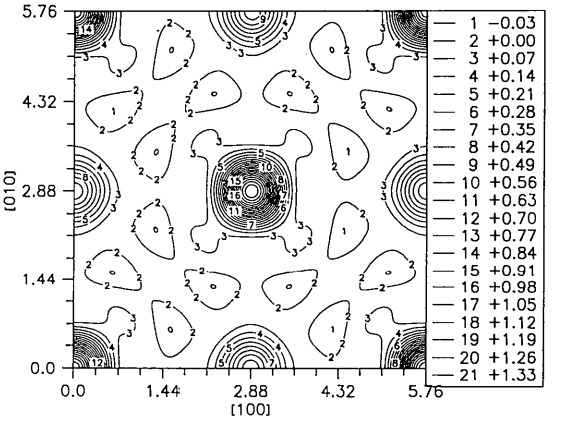

(*a*)

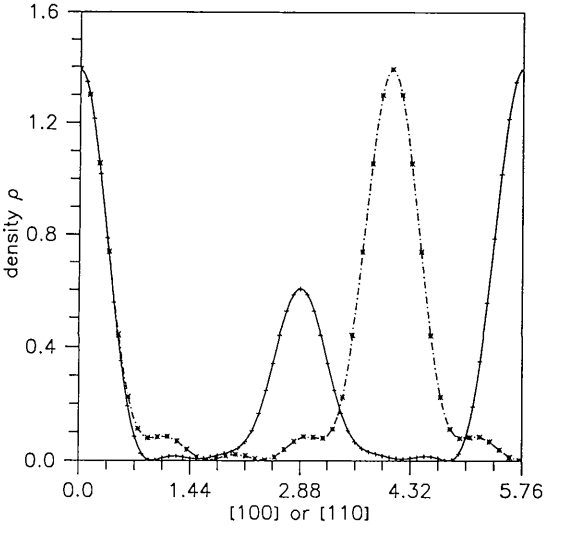

(*b*)

Fig. 1. (*a*) Contour map of the scattering-length density of KOD on the (001) plane by Fourier transformation, with the data of Table 1. (*b*) Density peaks along cuts in [110] (dash-dotted) and [100] directions. The D^+ distribution is seen as 'foothills'.

Table 2. *Model fit for the cubic structure of* KOH *and* KOD *according to equation* (2)

	$r_{OH/D}$	c_4	$\langle u^2\rangle_O$	$\langle u^2\rangle_{H/D}$	$\langle u^2\rangle_K$	χ^2	a (Å)
KOH	0.99	−3.2	0.093	0.099	0.135	25.0	5.78
KOD	0.97	−4.9	0.074	0.075	0.115	27.3	5.76

modelled by (Bleif, 1978; Press & Hüller, 1973; Seymour & Pryor, 1970):

$$\rho_H(\mathbf{r}) = [\delta(r - r_{OH})/4\pi r^2] \times \{1 + [c_4(x^4 + y^4 + z^4 - 3r^4/5)/r^4]\}, \quad (2)$$

representing spherical harmonics of the fourth degree compatible with cubic $m\bar{3}m$ symmetry. The coefficient giving the anisotropy of the hydrogen distribution, c_4, comes out rather large so that ρ_H has negative regions. Therefore, this only makes sense if folded with a DW factor which turns out to be the same as for oxygen, giving support to the dumb-bell model of the OH group. The DW factors are so large that higher-order expansion coefficients beyond the one used in (2) are not extractable from the data. The five parameters determined in the model fit are given in Table 2. The OH and OD distances are found to be just below 1 Å, which speaks against H or D bonding.

The good quality of this model fit is demonstrated in Fig. 2, where fitted and measured $F(hkl)$ as a function of distance from 000 in Q-space are plotted. In Fig. 3, the deuteron distribution from this model is shown. Postponing the discussion of details, we only point out that D^+ obviously avoids the [100] directions towards the alkali position. With this method, of course, the H distribution can also be extracted; it is very similar to the D distribution.

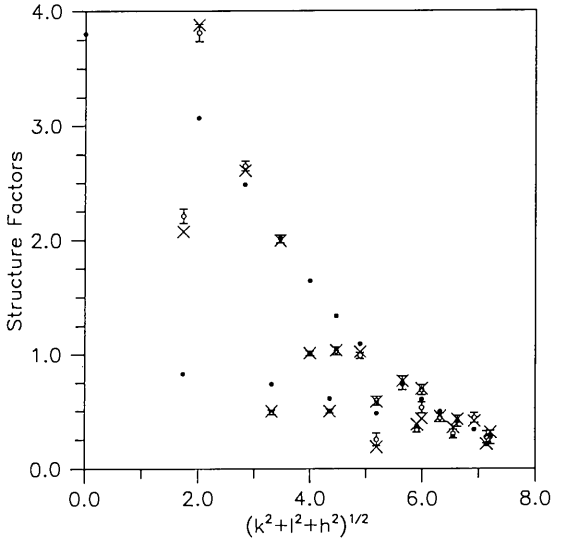

Fig. 2. Comparison of measured structure factors (o), with errors, of KOD with those resulting from the model fit (×) with equation (2). Also shown is the KO part from the model fit (•), to give a feeling for the D contribution.

3. Application of the MEM

The *MEED* program requires the N measured $|F(hkl)|$ values, the knowledge of the phases and the space group. Also, $F(000)$ and the lattice constant are input parameters and a uniform density in the cell is recommended as prior information. The numerical fit procedure according to the maximum-entropy principle stops when

$$\chi^2 = \sum_{n=1}^{N}(F_{obs} - F_{cal})^2/\sigma^2 = N. \quad (3)$$

The density is calculated iteratively starting from a prior density $\rho^{(0)}$:

$$\rho^{(\nu+1)}(\mathbf{r}_m) = \rho^{(\nu)}(\mathbf{r}_m)\exp\left(-\lambda\frac{\partial\chi^{(\nu)2}}{\partial\rho^{(\nu)}(\mathbf{r}_m)} + \mu_\nu\right). \quad (4)$$

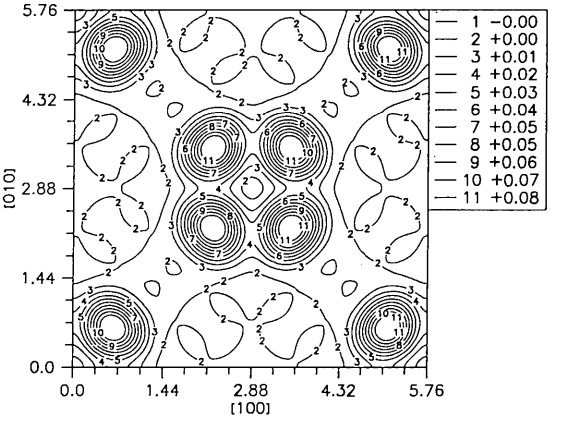

(*a*)

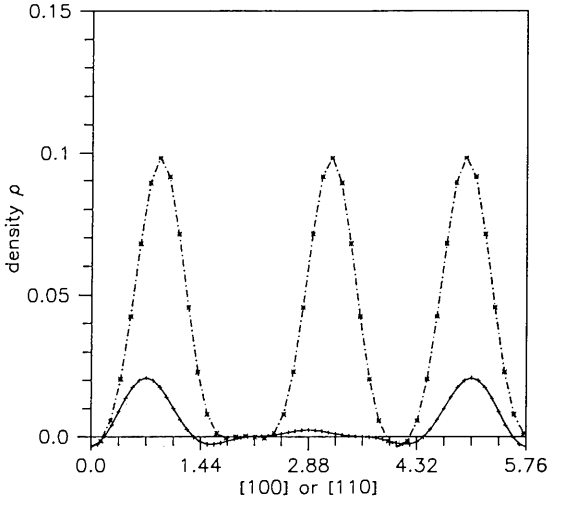

(*b*)

Fig. 3. (*a*) Contour map in the (001) plane of the D^+ density of KOD from the model fit, equation (2). The OD distance, also available as fit parameter (see Table 2), can be directly read off here. (*b*) Peak structure along cuts parallel to the cubic edge and the face diagonal. Note the weak artefacts between the peaks.

Note that the gradient for minimizing χ^2 appears in the exponent. The parameter λ controls the rapidity of the approach of condition (3) and the parameter μ ensures the density to be normalized such that $F(000)$ stays constant in the iteration procedure. The positions $\mathbf{r}_m$ are discrete, the minimum requirement for the number of grid points is apparently $N_g = 32 \times 32 \times 32$. The structure factors $F^{(\nu)}$ are calculated by an inverse Fourier transformation in each iteration:

$$F_{\text{cal}}^{(\nu)}(\mathbf{q}_n) = (a^3/N_g) \sum_{m=1}^{N_g} \rho^{(\nu)}(\mathbf{r}_m) \exp(-i\mathbf{q}_n\mathbf{r}_m) \qquad (5)$$

to obtain $\chi^{(\nu)2}$ using (3). If the iteration converges, one has at the end of a MEM density map $[\rho^{(\nu)} \rightarrow \rho_{\text{MEM}}]$. Evidently, a Fourier map and a MEM map of the scattering-length density cannot be the same, since, by (5), ρ_{MEM} yields all, including the unobserved structure factors, while the latter are ignored in the Fourier map since (1) is used. For a critical discussion, see Jauch (1994) and references therein.

In Fig. 4, the KOD density distribution obtained by the MEM is shown compared with Fig. 1. The structure factors fit well, even a little better than the model fit, but comparison of Fig. 1(*b*) with Fig. 4(*b*) reveals the difference in peak height and shape. As indicated, the difference in the density maps is not due to deviations between calculated and observed structure factors but to the unobserved structure factors. They are given values consistent with the MEM density; even if they are very small, there are many of them, working together to accommodate the *a priori* density. Therefore, such MEM

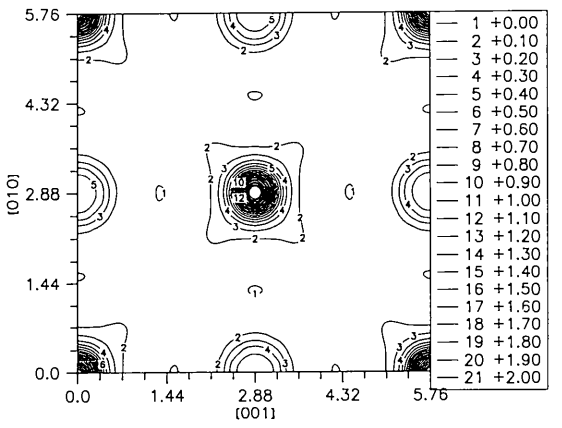

(*a*)

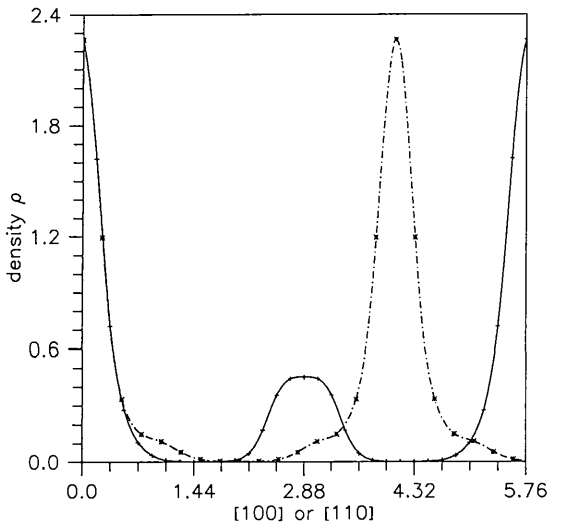

(*b*)

Fig. 4. (*a*) Contour map in the (001) plane for the KOD density from the straight application of the *MEED* program with 'zero bias'. (*b*) Peak structure in [110] and [100] directions. Note that the peak heights deviate from the Fourier result (Fig. 1*b*).

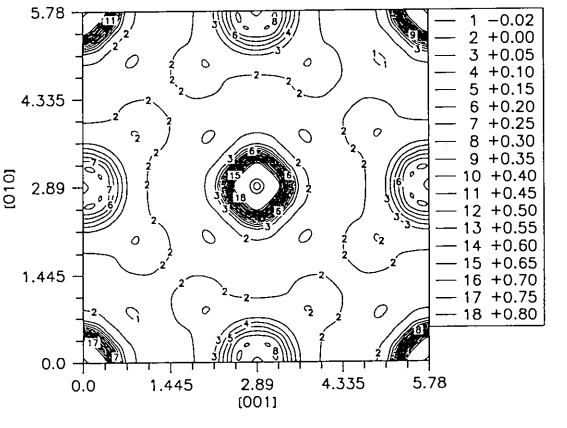

(*a*)

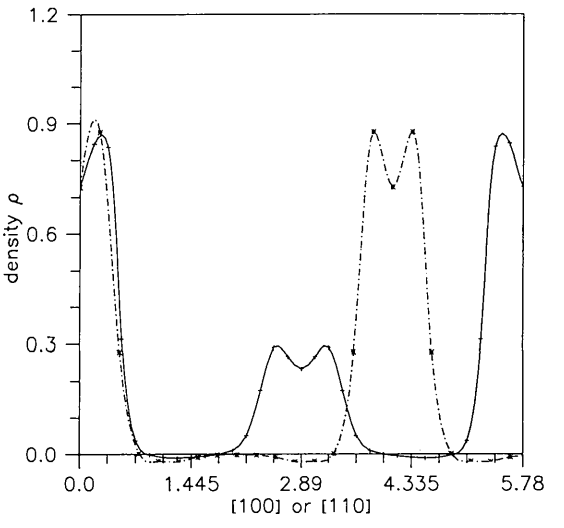

(*b*)

Fig. 5. (*a*) Contour map in the (001) plane for the KOH density from the naive application of the *MEND* program with 'zero bias'. (*b*) Peak structure in [110] and [100] directions. The split peaks are considered unacceptable.

maps tend to look smooth and the peak shapes may differ from Gaussians. Obviously, it is not fruitful at this point to argue which is the 'better' density.

One can obtain the list of the unobserved structure factors by running the *MEED* program again, with the calculated density as input, adding the list of F_{hkl} structure factors one is interested in, in addition to the measured ones, giving them a start value of zero, for example, and arbitrary but finite errors σ, but not starting the iteration routine.

In order to compare the corresponding density maps for KOH, one has to consider that hydrogen has a negative scattering length. The *MEED* program, requiring positive scattering densities (originally it was designed for X-ray data), can be modified to treat positive and negative scattering length densities separately. Sakata & Takata (1994) made the program *MEND* (maximum entropy for neutron diffraction) available to us, which we used to make sure that some peculiarities we found were not due to changes we made to the *MEED* program.

For KOH, one obtains the density shown in Fig. 5(*a*) if one starts again with a uniform density as before. Although the structure factors are well fitted, the density distribution with the split peaks is not acceptable, either for the positive density of KO or for KOH. The H density, giving only a tiny contribution (see Fig. 5*b*), cannot then be considered trustworthy.

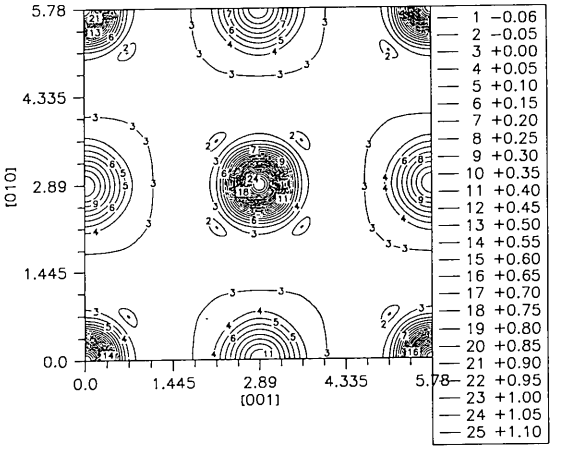

(*a*)

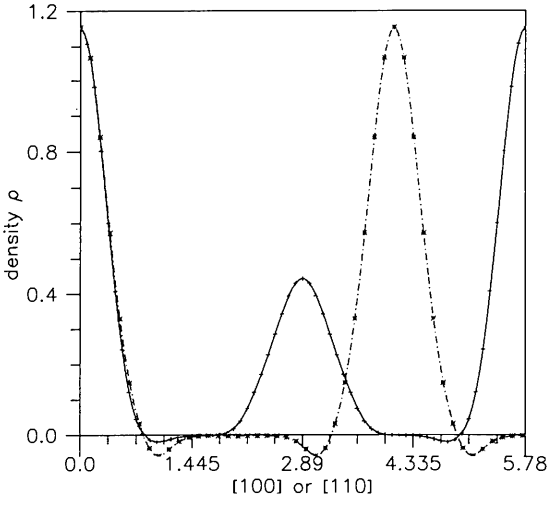

(*b*)

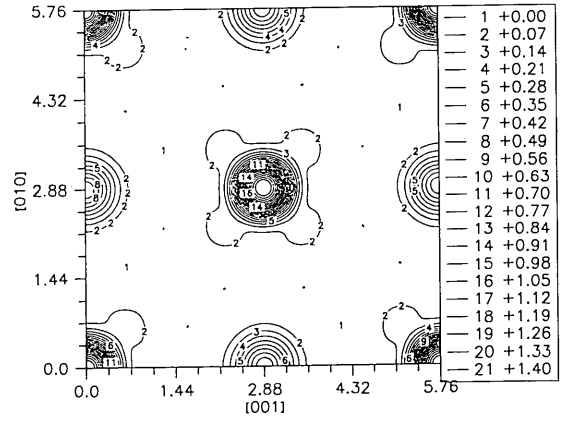

(*c*)

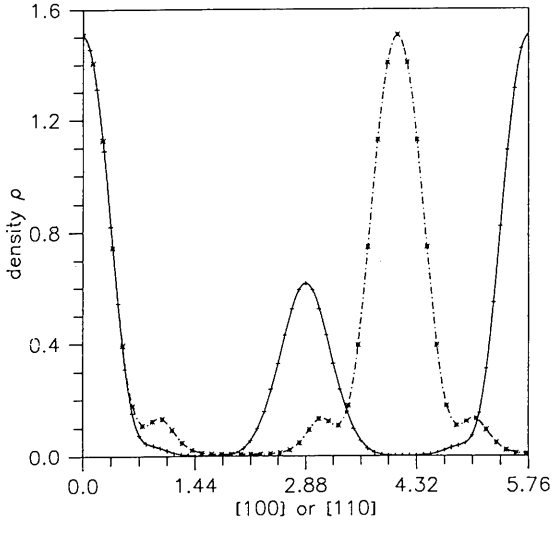

(*d*)

Fig. 6. (*a*) Contour map in the (001) plane for the KOH density after the sophisticated application of the *MEND* program (see text). (*b*) Peak structure in [110] and [100] directions for KOH. (*c*) Contour map in the (001) plane for the improved KOD density. (*d*) Peak structure in [110] and [100] directions for KOD. Note that the peak heights are now quite close to those of the Fourier result (Fig. 1*b*).

As explained before, the strange features in the KOH density map can be traced back to the unobserved reflections. The higher-indexed structure amplitudes are found to be unrealistically large (of such a size that some of them ought to have been observable) and, as in this case, they are all, except a few, associated with a negative sign which explains the reduction of the peak heights and the dips (see Fig. 3*b*). We decided not to devise an 'improvement' by artificially assigning zero or small values to the higher-order reflections, since it would change χ^2 completely, because there are many more unobserved than observed structure factors that have to be taken into account. χ^2 would then be dominated by contributions from estimated standard deviations (σ) of data one could not measure. Another method would also remove split peaks, namely setting the scattering lengths b_K, b_O and $b_{H/D}$ artificially higher, *e.g.* by 30%, but keeping the scaling of F_{obs}. Unfortunately, the surplus scattering density appears as a small almost uniform background in the unit cell which would interfere with the also extended and small H or D density we are looking for.

We chose a method of improvement by introducing a more suitable density distribution as prior information. Of course, the *MEED* KOD results do not serve this purpose since separated densities for KO and D are necessary as input. We proceeded in the following way: the (not so good) densities for KO and H from above were used, changing the sign of the H density, of course, as prior to fit the KOD data with *MEND*, yielding separated KO and D densities. This *a priori* density is sufficiently different from the KOD results expected, for example, from the Press–Hüller fit above, also due to differing DW factors and the different scattering lengths for D and H, so that enough freedom for the iteration procedure minimizing χ^2 is available. These results for the separated KO and D densities are then used as prior for the KOH fit with *MEND* shown in Figs. 6(*a*),(*b*). The KOD fit shown in Figs. 6(*c*),(*d*) is then obtained by repeating this procedure once more. Further repetitions seem to slowly degrade the quality of the fit. This procedure is *ad hoc* here, since we know of no general criteria for an optimal bias adapted to the numerical method. In this context, we point out a recent study

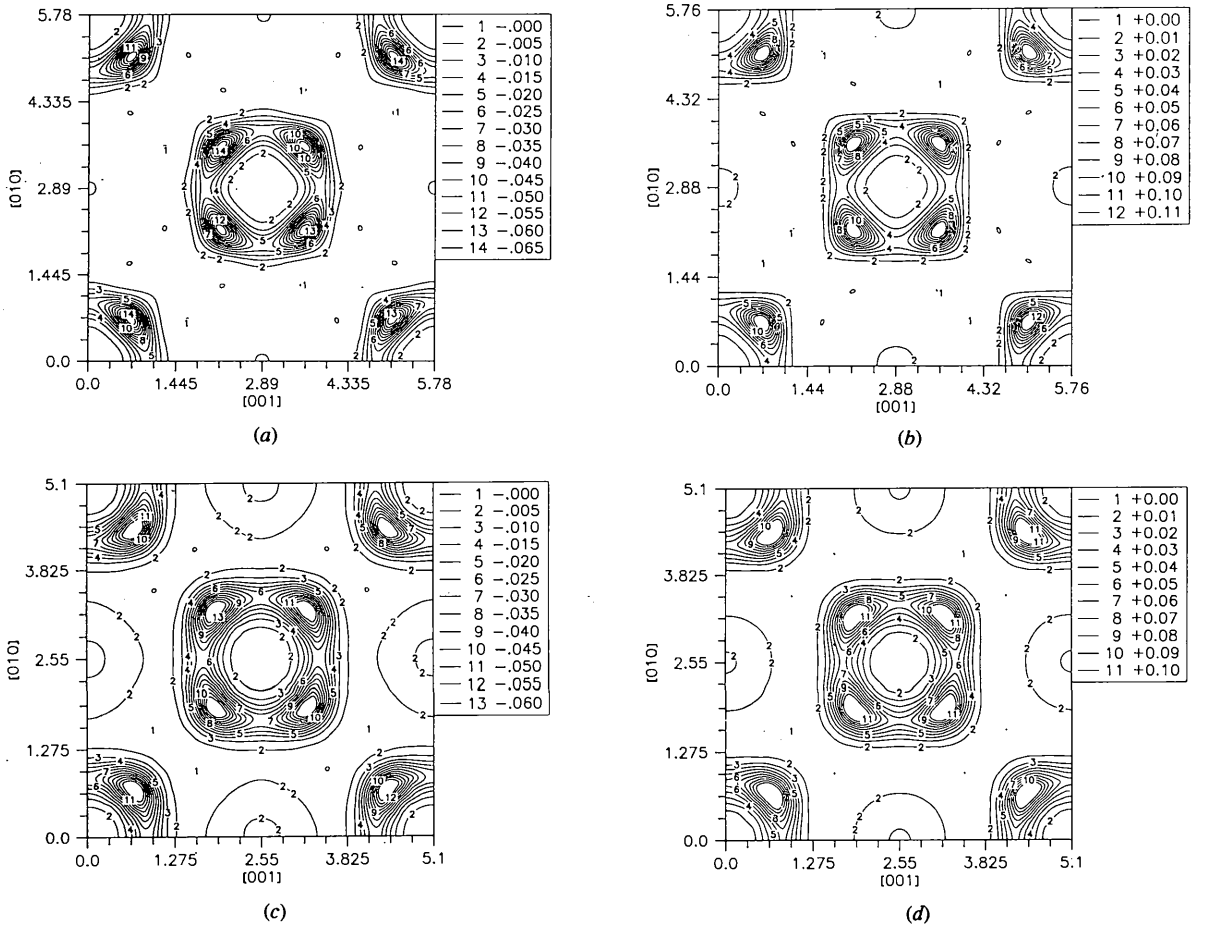

Fig. 7. (*a*) Density distribution of H^+ in KOH in the (001) plane. (*a*)–(*d*) all result from the sophisticated application of the *MEND* program as described in the text. (*b*) Density distrbution of D^+ of KOD in the (001) plane. (*c*) Density distribution of H^+ of NaOH in the (001) plane. (*d*) Density distribution of D^+ of NaOD in the (001) plane.

where all available knowledge has been used as a prior (Zheludev, Papoular, Ressouche & Schweizer, 1995).

The result, shown in Fig. 6, looks quite satisfactory: Figs. 1(*b*) and 6(*d*) should now be compared. In addition to the expected H density distribution, one has also obtained that for D, which at the beginning, according to the method, seemed impossible. The H and D distributions, also those for NaOH and NaOD produced in the same way, are shown in Fig. 7. An identical distribution to that from the modelling method is not expected but the agreement is not too bad (compare Fig. 8 with Fig. 3*b*). The OH or OD radii can now be directly read off from the respective density maps: for the potassium compounds it is 0.98 Å and for the sodium compounds 0.93 Å; the difference between H and D seems negligible.

Our results can be called 'model free' in the sense that we needed no explicit model for the prior density due to the lucky circumstances that data for the H as well as the D compounds are available and both are good 'models' of each other.

4. Discussion and concluding remarks

The procedure of fitting with the MEM is not so different from the conventional one, for example the Levenberg–Marquardt algorithm which we used in fitting the model discussed in §2. The main difference is that there are many more fit parameters than the three DW factors, the OH distance and the parameter c_4 for the H anisotropy. In principle, one has as many as the number of grid points N_g, reduced by symmetry though, but their number is still considerably larger than the number of observations. Therefore, the greater flexibility of the MEM fit is also a weakness: one needs additional *a priori* information. Usually, the starting density is taken as uniform. This did not work well for the high-temperature data of the alkali hydroxides. We found higher-order structure factors resulting from the MEM fit which should have been measurable because of their size; they appear to be artifacts of the fit.

We overcame the problem by using, without hoping for optimization, information from the deuterated compounds. We leave it to the reader to decide whether this method is still to be called 'model free'.

After this, we cautiously judge the quality of the MEM outcome for the H and D distribution, comparing Fig. 3, Fig. 7 and Fig. 8. Generally speaking, model and MEM fits reproduce the expected information such as anisotropy and radius of the hydrogen distribution. The differences between H or D, K or Na and O for the alkali hydroxides are 'strong' features and are clearly visible. Of course, the MEM does not directly yield an average OH or OD distance of DW factors. Weak features in the density distribution, like humps of very small size, occurred in both fitting procedures and cannot be trusted.

In conclusion, having data available which yield Fourier density maps with relatively small truncation errors, we had a guideline when applying the MEM to determine the H/D distributions. Only after giving up the uniform density as prior information, a quantitative agreement (within 10%) between MEM and Fourier maps was obtained and only then we considered the resulting H/D distribution as trustworthy.

We finally recommend the use of both methods to construct a model with physically interpretable parameters with the help of MEM, using the 'flat bias' to start with but checking the higher than measured F_{hkl}, using on the way (if necessary) preliminary models as priors for the maximum-entropy fits.

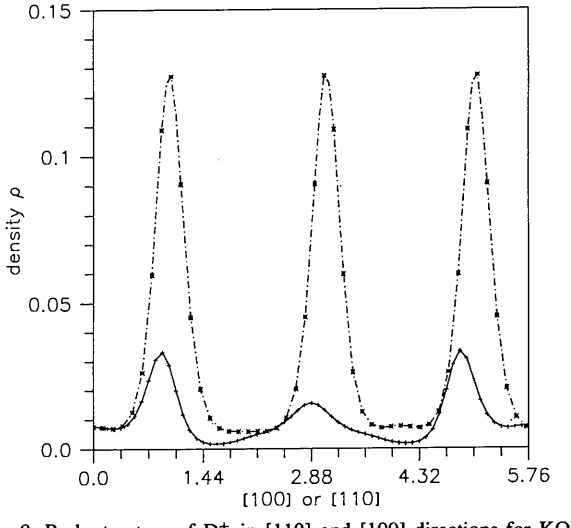

Fig. 8. Peak structure of D^+ in [110] and [100] directions for KOD using the *MEND* program as described in the text.

We are grateful to M. Sakata at the University of Nagoya for helpful advice in addition to letting us have his programs and to W. Jauch and H. J. Krappe, both of HMI Berlin, for very useful discussions.

References

BLEIF, H. J. (1978). Thesis, Univ. Tübingen, Germany.
BLEIF, H. J. & DACHS, H. (1982). *Acta Cryst.* A**38**, 470–476.
EL'KIN, B. SH. (1990). *Solid State Ionics*, **37**, 139–148.
JAUCH, W. (1994). *Acta Cryst.* A**50**, 650–652.
KABS, M. (1980). Thesis, Technische Univ. Berlin, Germany.
KARA, M. (1982). *Acta Cryst.* A**38**, 274–285.
KUMAZAWA, S., KUBOTA, Y., TAKATA, M. & SAKATA, M. (1993). *J. Appl. Cryst.* **26**, 453–457.
PAPOULAR, R. J. & GILLON, B. (1990). *Europhys. Lett.* **13**, 429–434.
PAPOULAR, R. J., PRANDL, W. & SCHIEBEL, P (1992). *Maximum Entropy and Bayesian Methods*, edited by C. R. SMITH, G. J. ERICKSON & P. O. NEUDORFER, pp. 359–376. Dordrecht: Kluwer Academic Publishers.
PRESS, W. & HÜLLER, A. (1973). *Acta Cryst.* A**29**, 252–256.
SAKATA, M., MORI, R., KUMAZAWA, S., TAKATA, M. & TORAYA, H. (1990). *J. Appl. Cryst.* **23**, 526–534.
SAKATA, M. & SATO, M. (1990). *Acta Cryst.* A**46**, 263–270.

SAKATA, M. & TAKATA, M. (1994). *MEND*. Nagoya Univ., Japan.
SATAKA, M., UNO, T., TAKATA, M. & HOWARD, C. J. (1993). *J. Appl. Cryst.* **26**, 159–165.
SEYMOUR, R. S. & PRYOR, A. W. (1970). *Acta Cryst.* B**26**, 1487–1491.
SMIT, J. G., DACHS, H. & LECHNER, R. E. (1979). *Solid State Commun.* **29**, 219–223.
ZHELUDEV, A., PAPOULAR, R. J., RESSOUCHE, E. & SCHWEIZER, J. (1995). *Acta Cryst,* A**51**, 450–455.

Acta Cryst. (1995). A**51**, 746–753

High-Q-Resolution X-ray Diffraction of Ordered Fe–Al Single Crystals

BY F. BLEY, F. LIVET, J. C. LEROUX AND J. P. SIMON
LTPCM (URA CNRS 29), ENSEEG-INPG, BP 75, 38402 Saint Martin d'Hères CEDEX, France

D. ABERNATHY, J. ALS-NIELSEN,* G. GRUEBEL AND G. VIGNAUD
European Synchrotron Radiation Facility, BP 220, 38043 Grenoble, France

G. DOLINO AND J. F. LEGRAND
Laboratoire de Spectrométrie Physique (URA CNRS 08), UJF BP 87, 38402 Saint Martin d'Hères CEDEX, France

D. CAMEL AND N. MENGUY†
Centre d'Etudes Nucléaires de Grenoble, 38041 Grenoble, France

AND M. PAPOULAR
Centre de Recherches sur les Très Basses Températures, CNRS, 38042 Grenoble, France

(*Received* 15 *February* 1995; *accepted* 22 *May* 1995)

Abstract

The use of synchrotron radiation in the study of ordering transitions is presented. The peak-profile measurements can be carried out with a resolution one order of magnitude better than with classical sources in all directions of the reciprocal lattice. In the case of Fe–Al alloys, the small-angle scattering techniques can be transposed in the vicinity of a Bragg superstructure peak, which provides information on the antiphase configuration of the ordered alloys. Moreover, the high brilliance of the undulator of the ESRF ID10 beamline enables coherent scattering experiments. The conditions necessary to record holograms from an inhomogeneous sample are discussed and some results are presented.

I. Introduction

The transitions occurring in $Fe_{(1-c)}Al_c$ alloys, $0.23 < c < 0.3$, have been extensively studied (Taylor & Jones, 1958; Morgand, Mouturat & Sainfort, 1968; Okamoto & Beck, 1971; Rimlinger, 1971; Swann, Duff & Fisher, 1972; Oki, Hasaka & Eguchi, 1973; Allen & Cahn, 1975, 1976, 1979; Köster & Gödecke, 1980; Kubaschewski, 1982; Anthony & Fultz, 1989; Inden & Pepperhoff, 1990; Park, Stephenson, Ludwig & Allen, 1992). At high temperatures, this system is in the A_2 phase, of b.c.c. structure, with a cubic cell of size a. With decreasing temperature, successively appear the B_2 phase of *sc* (CsCl) structure and the $D0_3$ phase, of f.c.c. stucture, with a doubled unit-cell parameter ($2a$).

In the units of the cubic cell (parameter a) of the A_2 phase, three types of Bragg peaks (hkl) can be distinguished, which are used to characterize the ordering:

$h + k + l = 2n$, h, k, l integers: fundamental peaks present in the three phases;

$h + k + l = 2n + 1$, h, k, l integers: superstructure peaks corresponding to both ordered phases;

$2h$, $2k$, $2l$ odd: characteristic of the $D0_3$ phase.

The careful study of the profile of the superstructure peaks provides information on the size and distribution of the domains of the various phases (Warren, 1969; Cheary & Grimes, 1972).

The transitions described here are essentially of second-order type, except close to the 24 at.% composition, where the convergence of the two transition lines and of the magnetic order leads to a complex phase diagram. Here, single crystals are used so that only the metastable coherent phase diagram has to be considered (Allen & Cahn, 1975).

* Present address: Risø National Laboratory, Roskilde, Denmark.
† Present address: Laboratoire MATOP, Université Saint-Jérôme, Case 151, 13397 Marseille CEDEX 20, France.